Impact of a ball with a bat or racket

Rod Cross
Physics Department, University of Sydney, Sydney, NSW 2006, Australia

(Received 27 October 1998; accepted 25 January 1999)

The collision of a ball with a baseball bat or a tennis racket is usually modeled in terms of rigid body dynamics, assuming that the hand exerts no impulsive reaction force on the handle during the collision. In this paper, a uniform aluminum beam was used as an idealized bat or racket, in order to examine both the rigid body approximation and the assumption that the hand force can be neglected. An aluminum beam was chosen so that its length and stiffness could easily be varied and so that the results could be compared with solutions for a flexible beam. It was found that rigid body models of beams, bats, or rackets are of limited use but the hand force can usually be neglected. The flexible beam model provides remarkably good agreement with experimental results and provides new insights into the dynamics of this type of collision, including the nature of the sweet spot.

I. INTRODUCTION

The collision between a baseball bat or a tennis racket and a ball is a nontrivial problem in mechanics that has been difficult to unravel experimentally and difficult to model theoretically. The simplest theoretical approach is to assume that the bat or racket is perfectly rigid and that the handle is not subject to any impulsive force during the collision.[1–4] The bat and ball speed after the collision can then be calculated from the conservation equations, in terms of the corresponding speeds before the collision, and an assumed or measured coefficient of restitution. This model is based on the assumption that the collision time is much shorter than the time taken for an impulse to propagate along the bat to the hand and back to the ball. Under these conditions, no information is transmitted to the ball regarding the impulsive force that may or may not be exerted on the handle. However, the model is not self-consistent in that (a) if the bat is perfectly rigid, and the hand exerts no force on the handle, then the end of the handle will part company with the hand during the collision, (b) the propagation time of a pulse along a very rigid bat will be much shorter than the collision time, and (c) if the bat is flexible and the handle remains undeflected during the collision, then the effective mass of the bat will be less than the actual mass since only part of the bat is involved in the collision. These shortcomings were recognized by Van Zandt,[5] who developed a numerical model to analyze the behavior of a flexible, nonuniform bat. A simplified version of Van Zandt's model, neglecting the shear force, is described below.

It has recently been shown,[6,7] for both a tennis racket and a baseball bat, that an impulse is transmitted to the hand while the ball is still in contact with the bat or racket. For a tennis racket, the ball remains in contact with the strings for about 4 or 5 ms, and the impulse takes about 1.5 ms to reach the hand. For a baseball bat, the ball remains in contact with the bat for about 1.0–1.5 ms, depending on the relative speed of the bat and ball, and the impulse takes about 0.6 ms to reach the hand. The impulse reflected from the hand therefore arrives back at the ball at a time when the ball is about to lose contact with the bat or racket. The handle motion is strongly affected by the impulsive force exerted by the hand during the collision, but the question remains as to whether the ball is affected to any significant extent.

The experiment described in this paper was designed to investigate both the rigid body approximation and the assumption that the impulsive reaction force of the hand can be neglected. For this purpose, a uniform aluminum beam was used as an idealized bat or racket so that (a) it could be more easily and more accurately instrumented, (b) its length and stiffness could easily be varied, and (c) it could be more easily analyzed in terms of conventional beam theory. If such a beam is suspended horizontally by vertical strings attached to each end, and if a ball impacts at normal incidence at its center of mass (c.m.), then the effective mass of the beam would ideally be equal to the actual mass of the beam. However, if it bends in the middle and is sufficiently long that it remains undeflected at each end during the impact, then the effective mass will be less than the actual mass. The effective mass at any point along the beam can be defined by the relation $M_E = F/a$, where F is the force applied at that point and a is the acceleration of that point. The effective mass of a short beam, clamped at both ends, should be much larger than the actual mass of the beam. It would be infinite if the beam were infinitely stiff and attached to an infinite mass at each end. However, if the beam is sufficiently long and sufficiently flexible, it is conceivable that the effective mass for an impact at any point well removed from either end of the beam will be independent of the impact location or the beam length or the method of support at the ends.

II. BEAM THEORY

The equation of motion for a beam subject to an external force, F_0 per unit length, has the form[8,9]

$$\rho A \frac{\partial^2 y}{\partial t^2} = F_0 - \frac{\partial^2}{\partial x^2}\left(EI \frac{\partial^2 y}{\partial x^2} \right), \tag{1}$$

where ρ is the density of the beam, A is its cross-sectional area, E is Young's modulus, I is the area moment of inertia, and y is the transverse displacement of the beam at coordinate x along the beam. This equation neglects the shear force which is of minor significance for short wavelength modes but is negligible for long wavelength modes.[5,8] For a uniform beam of mass M and length L, numerical solutions of Eq. (1) can be obtained by dividing the beam into N equal segments each of mass $m = M/N$ and separated in the x direction by a distance $s = L/N$. An impacting ball may exert a force acting

over several adjacent segments, depending on the ball diameter and the assumed number of segments. For simplicity it was assumed that the ball impacts on only one of the segments, exerting a time-dependent force, F. The equation of motion for that segment (the nth segment) is obtained by multiplying all terms in Eq. (1) by s, in which case

$$m\frac{\partial^2 y_n}{\partial t^2}=F-(EIs)\frac{\partial^4 y_n}{\partial x^4}, \tag{2}$$

assuming that the beam is uniform so that E and I are independent of x. The equation of motion for the other segments is given by Eq. (2) with $F=0$. The boundary conditions at a freely supported end are given by $\partial^2 y/\partial x^2=0$ and $\partial^3 y/\partial x^3=0$. The boundary conditions at a rigidly clamped end are $y=0$ and $\partial y/\partial x=0$.

If it is assumed that the ball behaves as a simple spring, with a spring constant k_b, then the equation of motion for the ball is given by

$$m_b d^2 y_b/dt^2=-F=-k_b(y_b-y_n), \tag{3}$$

where m_b is the ball mass, y_b is the displacement of the ball, and y_b-y_n is the compression of the ball. It is assumed that at $t=0$, $y_b=0$, $y=0$ for all beam segments, the beam is initially at rest and that $dy_b/dt=v_1$. The subsequent motion of the ball and the beam was evaluated numerically using finite difference forms of Eqs. (2) and (3), as described in the Appendix. These results were used to determine the rebound speed of the ball, v_2, and the apparent coefficient of restitution (ACOR), $e=v_2/v_1$. In normal play, a bat or racket is swung toward the ball and is not normally at rest at the moment of impact. The resulting outgoing speed of the ball is easily related to laboratory measurements of the ACOR for an initially stationary bat or racket, using a simple coordinate transformation, as described by Brody.[4]

Analytical solutions of Eq. (1) for a uniform beam can be obtained when $F_0=0$ by assuming solutions of the form $\exp[i(kx-\omega t)]$, in which case one obtains the dispersion relation

$$k^4=m_0\omega^2/(EI), \tag{4}$$

where ω is the angular frequency, k is the wave number, and m_0 is the beam mass per unit length. For a rectangular cross section beam, $I=ba^3/12$ where b is the width of the beam and a is the thickness in the direction of vibration. The mass per unit length is $m_0=\rho ab$. From these relations it is easy to show that the phase velocity, $v_p=\omega/k$, and the group velocity, $v_g=\partial\omega/\partial k$, are given by $v_p=(Ea^2\omega^2/12\rho)^{1/4}$ and $v_g=2v_p$. For aluminum, $E=7\times10^{10}\,\mathrm{N\,m^{-2}}$ and $\rho=2700\,\mathrm{kg\,m^{-3}}$, so $v_g=2v_p=192.2(af)^{1/2}$ where $f=\omega/(2\pi)$.

The mode frequencies of a freely supported, rectangular cross-section beam are given by[8,9]

$$\omega=\frac{G^2 a}{L^2}\sqrt{E/(12\rho)}, \tag{5}$$

where $G=kL=4.730$, 7.853, 10.996 for the first three modes. If the beam is clamped at one end then $G=1.875$, 4.694, 7.853, 10.996 for the first four modes. The clamped beam mode periods for the beams studied in this experiment are summarized in Table I. The corresponding periods for a freely supported beam are very similar, except for the fact that the ''diving-board'' mode (with $G=1.875$) is absent.

Table I. Aluminum beam parameters.[a]

L (m)	a (mm)	M (g)	T_0 (ms)	T_1 (ms)	T_2 (ms)	T_3 (ms)
0.3	6	156	18.2	2.91	1.04	0.53
0.6	6	311	73.0	11.6	4.16	2.12
1.1	6	570	245	39.1	14.0	7.13
1.1	10	950	147	23.5	8.39	4.28
1.8	6	933	657	104.8	37.4	19.1

[a]Mode periods are given for the first four modes of a beam clamped at one end.

III. BALL LOSSES

Solutions of Eqs. (2) and (3) overestimate the ACOR due to the neglect of energy dissipation in the ball. A correction factor for ball losses was obtained from measurements of the ACOR when the ball impacted on one of the heavy steel supports used to clamp the beam. For such an impact, $e=0.85\pm0.01$, indicating that a fraction $(1-e^2)=0.28$ of the incident ball energy is dissipated in the ball. This was confirmed by measurements of the ratio of the rebound height to the drop height when the ball was dropped on a solid floor.

A simple correction for ball losses can therefore be obtained by multiplying the theoretical values of e by 0.85. Alternatively, ball losses can be incorporated directly in Eqs. (2) and (3) by allowing for hysteresis in the ball. The compression and expansion phases of a bouncing ball are known to obey different force laws.[10,11] The area enclosed by a force versus compression curve, for a complete compression and expansion cycle, is equal to the energy dissipated in the ball. A realistic model is obtained by assuming that $F=k_1x^m$ during the compression phase and $F=k_2x^n$ during the expansion phase, where x is the ball compression. A typical hysteresis curve is shown in Fig. 1. Since the two values of F are equal at maximum compression, x_0, k_2 is given by $k_2=k_1x_0^{m-n}$. For this model, the energy loss in the ball, E_b, is given by

$$E_b=\oint F\,dx=\frac{(n-m)k_1x_0^{(m+1)}}{(m+1)(n+1)}. \tag{6}$$

For an impact on a rigid surface, the maximum potential energy stored in the ball can be equated to the incident kinetic energy of the ball, provided there is no energy loss during the compression phase. In this case, the ball loss is the only energy loss, so

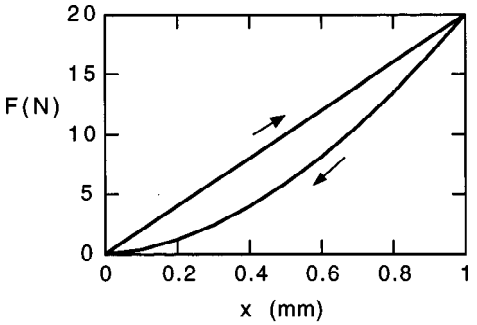

Fig. 1. Dynamic hysteresis curve for a superball with $k_1=2\times10^4\,\mathrm{N\,m^{-1}}$, $m=1.0$, $e=0.85$, and $n=1.768$.

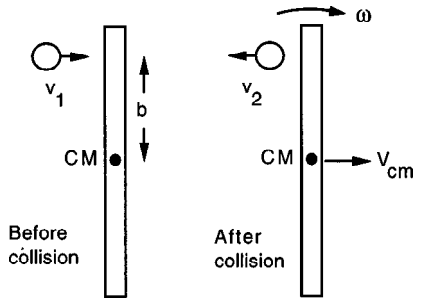

Fig. 2. Collision of a ball with a freely suspended rigid bat initially at rest.

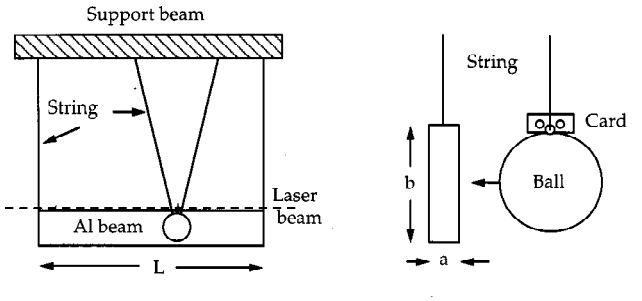

Fig. 3. Experimental arrangement used to measure the incident and rebound speeds of a ball impacting on an aluminum beam.

$$1-e^2=\frac{E_b}{0.5m_bv_1^2}=\frac{(n-m)}{(n+1)}. \tag{7}$$

Equation (7) indicates that e is independent of ball speed. In fact, it is known that e decreases slightly as the ball speed increases, in which case n and m are slowly varying functions of v_1. The effect is relatively small[11] and is of no concern in this paper. In this experiment, a superball was used in order to minimize the energy loss in the ball itself, and the incident ball speed was not varied. Previous measurements[11] have shown that a good approximation for the dynamic compression of a superball is given by $m=1$, in which case $e^2=2/(n+1)$. For the ball used in this experiment, appropriate parameters are given by $k_1=2\times10^4\,\mathrm{N\,m^{-1}}$, $e=0.85$, $m=1.0$, and $n=1.768$. Equations (2) and (3) can therefore be modified so that $F=k_1(y_b-y_n)$ during the compression phase, and $F=k_2(y_b-y_n)^{1.768}$ during the expansion phase. The results of such a calculation are presented below.

IV. RIGID BODY APPROXIMATION

For a sufficiently short or a sufficiently stiff bat, the collision between a bat and a ball can be analyzed using a rigid body approximation, as illustrated in Fig. 2. If there is no external reaction force from the hand, and if the bat is initially at rest, then conservation of linear and angular momentum is described by the relations

$$m_bv_1=MV_{\mathrm{c.m.}}-m_bv_2 \tag{8}$$

and

$$m_bv_1b=I_{\mathrm{c.m.}}\omega-m_bv_2b, \tag{9}$$

where M is the bat mass, $V_{\mathrm{c.m.}}$ is the recoil speed of the center of mass (c.m.) of the bat, $I_{\mathrm{c.m.}}$ is the moment of inertia of the bat about its c.m., ω is the angular velocity of the bat after the collision, and b is the impact parameter. For a uniform bat of length L, $I_{\mathrm{c.m.}}=ML^2/12$. Conservation of energy is described by

$$m_bv_1^2=m_bv_2^2+MV_{\mathrm{c.m.}}^2+I_{\mathrm{c.m.}}\omega^2+2E_c, \tag{10}$$

where E_c is the energy dissipated in the ball plus the energy stored as vibrational energy in the bat. The vibrational energy is eventually dissipated in the bat, or in the hands, well after the collision is over. Inclusion of a vibrational loss term allows one to relax the assumption that the bat is perfectly rigid, but rigid body dynamics alone does not provide any clues as to the magnitude of E_c. The vibrational losses must be determined experimentally or by a flexible bat analysis. The solution of Eqs. (8)–(10) is given by

$$e=\frac{v_2}{v_1}=\frac{[1-f(1+R)]^{1/2}-R}{1+R}, \tag{11}$$

where $f=2E_c/(m_bv_1^2)$ is the fractional energy loss, $R=m_b/M_E$, and

$$M_E=\frac{M}{(1+Mb^2/I_{\mathrm{c.m.}})} \tag{12}$$

is the equivalent mass of the bat as defined in Sec. I. Equation (11) is therefore the same as that for a head-on inelastic collision between point masses m_b and M_E. The equivalent mass is equal to the actual mass for an impact at the c.m. where $b=0$, and decreases toward the end of the bat. At the end of the bat, where $b=L/2$, $M_E=M/4$. Solutions of Eq. (11) are given below to compare with the flexible bat solutions and with the experimental data.

V. EXPERIMENTAL ARRANGEMENT

The arrangement used in this experiment is shown in Fig. 3. A rectangular cross-section aluminum beam of width 32 mm was supported horizontally, either by a 1.2 m vertical length of string attached to each end or by clamping one end to a rigid support. A 36-mm-diam, 42-g superball was mounted, as a pendulum bob, at the apex of a V-shaped string support, so that it could impact the beam horizontally and at right angles to the beam. Impacts toward one edge of the beam caused it to rotate and vibrate about the long axis, resulting in a significant reduction in the ball rebound speed. Consequently, care was taken to ensure that the ball impacted on the center-line along the beam, 16 mm from each edge. This arrangement provided good reproducibility as well as a simple and accurate means of both controlling and measuring the ball speed. For the latter purpose, a small (5 mm×15 mm) rectangular card was glued to the top of the ball. A He–Ne laser beam was directed parallel to the beam so that it could pass sequentially through two small holes in the card, 10 mm apart. The laser beam was detected using a photodiode. From these data, measurements were obtained of the ACOR as a function of impact location along the beam.

It is difficult to suspend a beam so that both ends are totally free. The method of supporting the beam at each end by a length of string or fine wire is a good approximation, since the restoring force on the beam due to the string support is much smaller than the impulsive force of the ball acting on the beam, at least for small horizontal displace-

ments of the beam. In this experiment, the ball was incident at low speed, about 1 ms^{-1}, the impact duration was about 4 ms, and the end of the beam deflected horizontally by less than 4 mm during the impact. The peak impact force was about 15 N, and the peak horizontal restoring force due to the string support was about 0.01 N.

Two piezo ceramic disks were mounted on the beam with adhesive tape in order to monitor the impact duration and the propagation delay of the transverse wave along the beam. The disks were 25 mm in diameter, 0.3 mm thick, and had a mass of only 1.9 g so they did not have any significant effect on the behavior of the beam. However, measurements of e were obtained without the disks in place since a direct impact with a disk acted to decrease e by about 5%. The disks were connected to 10-$M\Omega$ oscilloscope probes using very light leads taped to the beam in order to avoid any spurious response due to independent motion of the leads. The output signals from the piezo disks were recorded on a digital storage oscilloscope. A direct impact of the ball on a piezo disk provides a measurement of the force of the ball on the disk. If the ball impacts at some other point on the beam, then the output of a piezo attached at any point P along the beam provides a measurement of the local acceleration of the beam at point P. For some experiments, the probe output was connected to an RC integrator of time constant 1.0 s in order to monitor the local velocity of the beam.

VI. WAVE SPEED MEASUREMENTS

When a ball impacts on a beam, it excites a broad spectrum of frequency components from zero frequency up to about $1/\tau$, where τ is the duration of the impact. The force waveform acting on the beam is approximately a half sine wave, in which case the amplitude of the spectrum peaks at zero frequency and drops to zero at $f=1.5/\tau$. In theory, the impulse observed at any point on the beam, shortly after the impact, should contain frequency components up to about $1.5/\tau$. In practice, the highest frequency components are too small in amplitude and too heavily damped to be observed. All components are dispersed along the beam since the high frequency components propagate faster than the low frequency components. Results obtained with an aluminum beam of length 1.8 m, width $b=32$ mm, and thickness $a=6$ mm are shown in Fig. 4. The beam was freely suspended in a vertical orientation by a length of string attached to the top end, and struck 10 cm from the bottom end by the 42-g superball. The velocity waveform at each end of the beam was detected by a piezo disk mounted at each end of the beam on the side opposite the impact side. The piezo at the bottom end therefore responded almost immediately to the impact and, after a significant delay, to the signal reflected from the top end of the beam.

As shown in Fig. 4, the high frequency components arrive first and are relatively small in amplitude. The low frequency components propagate at a lower speed and are larger in amplitude. The lowest frequency components arrive at a time when the high frequency components have completed two or three round trips along the beam. The time delay between the initial impact and the arrival of any given peak in the dispersed impulse provides a measurement of the group velocity. For example, the second peak in Fig. 4(b) arrives after a delay of about 22 ms and is centered at a frequency of around 140 Hz. The velocity of this peak is therefore about 160 ms^{-1} and the expected group velocity at 140 Hz is 176 ms^{-1}. However, the frequency is not sufficiently well-defined to provide an accurate estimate of the group velocity for this data. Better measurements of the dispersion relation are obtained from measurements of the vibration periods, which were found to agree closely with the results given in Table I.

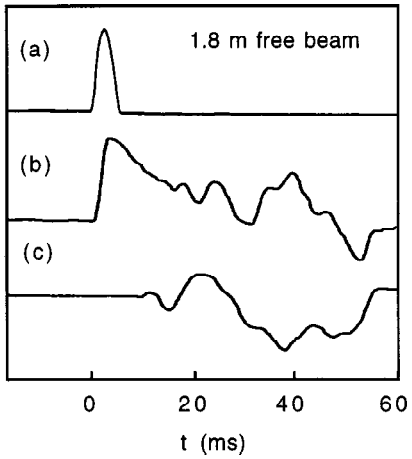

Fig. 4. Measurements of wave propagation along an aluminum beam ($L=1.8$ m, $a=6$ mm, $b=32$ mm) when a superball impacts at one end, showing waveforms of (a) the impact force on the beam, (b) the beam velocity at the impact end, and (c) the beam velocity at the other end of the beam.

Numerical solutions of Eqs. (2) and (3) for this impact are shown in Fig 5. The solutions are generally consistent with the observed waveforms but there is no wave damping in (2) or (3), so the high frequency components feature more prominently than is observed. An interesting feature of the solutions is that the beam velocity near the impact point peaks at the end of the impact and then decays toward zero in an exponential fashion, as observed. This feature implies that most of the impact energy is absorbed near the impact point and is then redistributed along the beam over a relatively long time period due to the low group velocity of the low frequency components of the impulse.

VII. ACOR MEASUREMENTS

Measurements of the ACOR, and the corresponding theoretical estimates of the ACOR, are presented in Fig. 6 for aluminum beams with $a=6$ mm, $b=32$ mm, and $L=30$, 60, and 110 cm. Results for a thicker beam, with $a=10$ mm, b

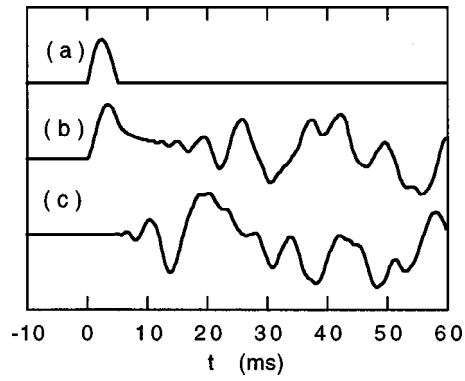

Fig. 5. Solutions of Eqs. (2) and (3) for the impact shown in Fig. 4, with corresponding waveforms (a), (b), and (c).

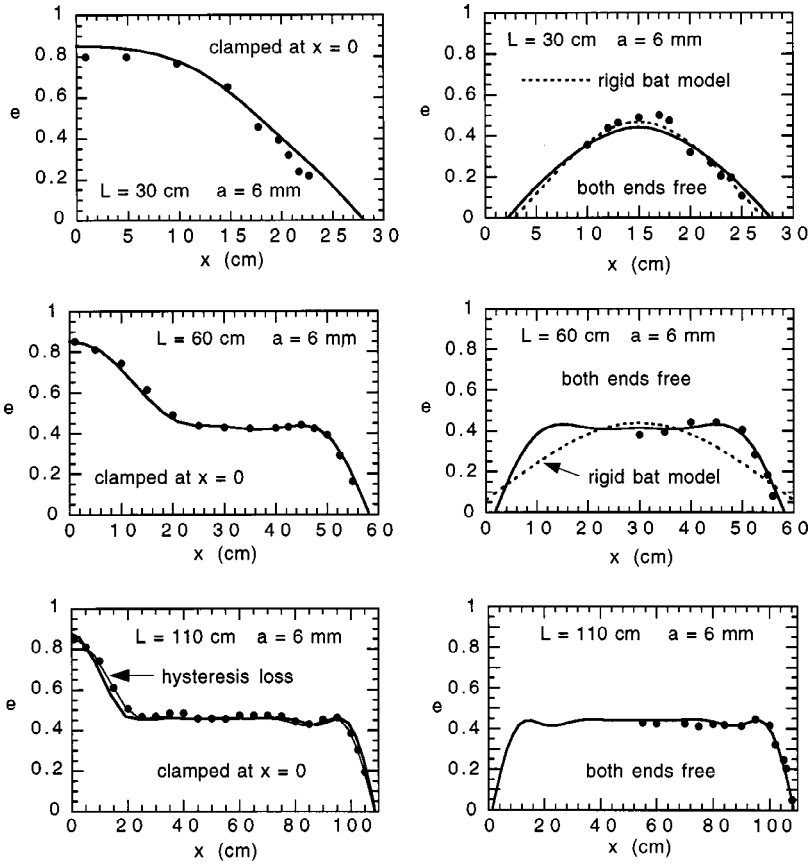

Fig. 6. A comparison of theoretical and experimental values of ACOR for the 6-mm-thick aluminum beams. Experimental data are represented by closed dots. The solid curves represent numerical solutions of Eqs. (2) and (3), multiplied by 0.85 to account for ball losses. The thin line curve for the 110-cm clamped beam is computed with hysteresis losses included in the dynamics. The dashed curves for the freely supported beams are solutions for a rigid body model with a loss fraction $f=0.6$ for the 60-cm beam and $f=0.2$ for the 30-cm beam.

$=32$ mm, and $L=110$ cm are shown in Fig. 7. The theoretical estimates were obtained using a simple correction factor of 0.85 for ball losses. The spring constant was taken as $k_b=2\times10^4\ \mathrm{N\,m^{-1}}$ to be consistent with the observed impact duration, about 4.2 ms. An alternative theoretical value of e, allowing for dynamic hysteresis losses in the ball, is shown for the $L=110$ cm clamped beam. The alternative solution (shown as a thinner line) is very similar to the first solution but provides slightly better agreement with the experimental data.

Apart from a few minor discrepancies, agreement between the theoretical and experimental values of e is remarkably good. Higher than expected values of v_2 can result if the ball rotates slightly on impact, thereby reducing the effective width of the card and the effective distance between the holes in the card. For the 30-cm clamped beam, significantly higher values of v_2 were observed for impacts close to the free end, due to the fact that the beam vibrated and struck the almost stationary ball soon after the initial impact. These double-impact results are not included in Fig. 6. Results obtained for the lighter 30-cm free beam were not as accurate or as reproducible as the other beams, since small misalignment errors had a larger effect on rotation of the beam about the long axis.

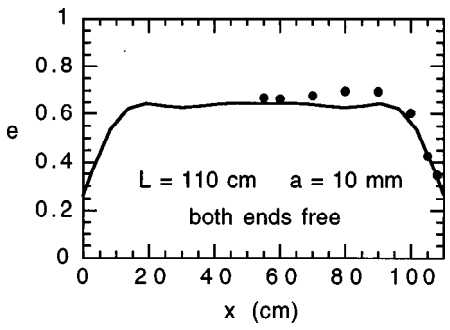

Fig. 7. A comparison of theoretical and experimental values of ACOR for the 10-mm-thick aluminum beam. Solutions of Eqs. (2) and (3) are multiplied by 0.85 to account for ball losses.

The results in Fig. 6 show very clearly that, for a sufficiently long beam, (a) the impact of a ball near one end of a beam is not affected by the length of the beam or the method of support at the other end and (b) the ACOR for an impact anywhere along the central section of a beam is independent of the impact location and is not affected by the length of the beam or the method of support. For the longer 6-mm-thick beams, the ACOR remains constant at $e=0.45\pm0.02$ along the beam up to a point about 15 cm from each end. This result implies that the rebound speed is affected only if the impulse reflected off one end arrives back at the impact point within the 4.2-ms period of the impact. This places an upper limit on the propagation speed, of 30 cm/4.2 ms$=71\ \mathrm{ms^{-1}}$, of the significant frequency components. In other words, only those frequency components with a propagation speed of 71 $\mathrm{ms^{-1}}$ or less have any significant influence on the rebound speed. For a 6-mm-thick beam, the group velocity is 71 $\mathrm{ms^{-1}}$ at $f=22$ Hz or $T=1/f=45$ ms.

There is no simple formula that predicts that 22 Hz is a critical frequency, but most of the energy of the impulse is contained in the low frequency components. The dynamics of the situation are illustrated in Fig. 8, which shows the theoretical beam deflection, for a freely supported beam, at equal time increments during and shortly after the impact.

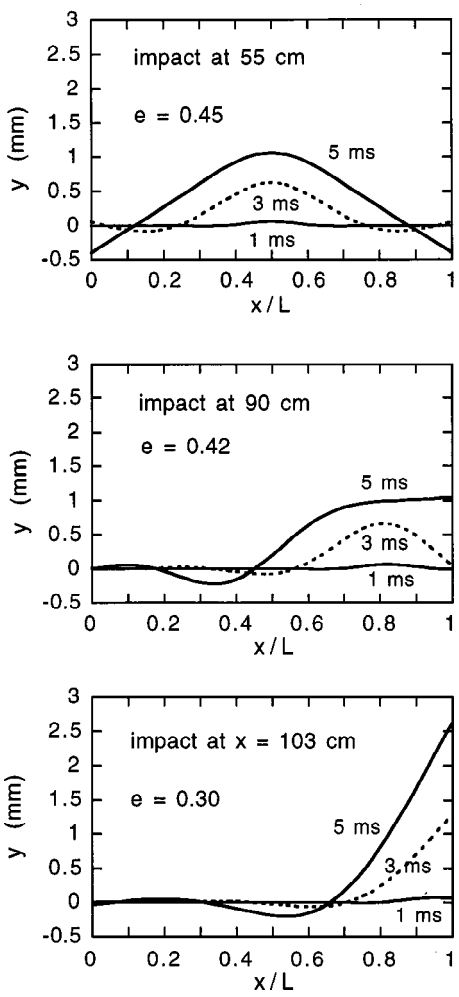

Fig. 8. The y displacement of a freely suspended beam vs x/L at times $t=1$, 3, and 5 ms after the initial impact (at $t=0$) for a beam with $L=110$ cm, $a=6$ mm, $b=32$ mm. A 42-g superball impacts normally on the beam at $x=55$ cm, $x=90$ cm, or $x=103$ cm. The ball is incident in the positive y direction at an initial speed $v_1=1.0\,\mathrm{ms}^{-1}$ and rebounds in the negative y direction at speed $v_2=ev_1$. The modeled impact duration is approximately 4.2 ms for each of the three impacts.

An impulse propagating toward a free end is reflected without phase reversal, so the beam moves further away from the ball, thereby reducing the rebound speed. A pulse propagating toward a clamped end is reflected with a phase reversal, sending the beam back toward the ball, thereby increasing the rebound speed. The reflected pulse has no effect on the ball if the ball rebounds before the reflected pulse reaches the ball. The theoretical results in Fig. 8 show that the beam deflection at the impact point, during the impact, is essentially the same for impacts at $x=55$ cm or $x=90$ cm, indicating that the pulse reflected at $x=110$ cm does not have a significant influence on the impact. However, for an impact at $x=103$ cm, the reflected pulse acts to deflect the beam away from the ball during the impact, thereby reducing the ACOR significantly.

An attempt to fit the $L=60$ cm, $a=6$ mm free beam data using a rigid body approximation is shown in Fig. 6. The dashed curve is the solution of Eq. (11), assuming that the beam mass $M=311$ g (i.e., its actual mass) and that $f=0.6$. The fit is not good, and is even worse for other assumed values of f. Similar poor fits can be obtained if one assumes that the beam mass is less than the actual mass and that f is less than 0.6. The problem with the rigid body model is that there is no solution of Eq. (11) where e remains constant over the central section of the beam. A rigid body solution could be ''forced'' to fit the data if f is allowed to vary with x, but the flexible beam solution is obviously superior. Nevertheless, a ''forced'' fit provides a valid measure of the fractional energy loss, f, consistent with the conservation equations. The fractional energy loss is about 0.6 in the middle of the 60-cm free beam and also at $x=3.8$ cm and $x=56.2$ cm, but it is different at other points along the beam.

A much better rigid body fit can be obtained for the $L=30$-cm free beam since the propagation time of an impulse along the beam is then comparable to the duration of the impulse. A good fit is obtained by assuming that the beam mass is its actual mass and that $f=0.2$, indicating that the ball loss is the main energy loss and that the fractional energy loss is less than that for an impact on a hard surface. This fit is shown by the dashed curve for the 30-cm free beam. The solid curve is the solution of Eqs. (2) and (3) with a correction factor of 0.85. An even better fit is obtained if the correction factor is changed to 0.89, in which case it is almost identical to the rigid body solution. This correction factor is consistent with the fact that the loss fraction $f=1-e^2=0.2$. One can conclude from these data that the rigid body approximation yields reliable results only if the duration of the impulse is longer than the vibration period of the fundamental mode of the freely supported beam.

VIII. ENERGY BALANCE

The results shown in Fig. 8 highlight a significant difference between the flexible and rigid body models of a beam. If one end of a beam is in motion while the other end is at rest, then the linear and angular velocities of the beam are not well defined. Spatially averaged linear and angular velocities can be defined, but these averages contain time-varying vibrational components that are not easily distinguished from the time-independent components until well after the collision is over. In the ideal case of a lossless, freely supported beam, and at times well after the collision, each point in the beam will then have a well-defined time average velocity or dc component, and a well-defined vibrational or ac component. The dc components must obey the conservation equations for linear and angular momentum, and the system as a whole must conserve energy, as described by the rigid body relations in Sec. IV.

Experimentally, it is observed that e is independent of the impact parameter for impacts sufficiently well removed from either end of the beam. Under these conditions, and for any given freely supported beam, it can be seen from (8) and (9) that $V_{\mathrm{c.m.}}$ is independent of b and ω is directly proportional to b. Equation (10) indicates that as b increases, E_c must decrease by the same amount as the rotational energy increases, in order to conserve energy. The distribution of the initial energy for an impact on the $L=110$-cm, $a=6$-mm free beam, is shown in Figs. 9 and 10 for impacts at $x=55$ cm and $x=90$ cm, respectively. The curve labeled ''Ball PE'' is the energy stored in the ball as a result of its compression plus the energy dissipated in the ball as a result of hysteresis losses. The ''Beam KE'' is the total instantaneous kinetic energy of all beam segments. The ''Beam PE'' is the strain energy arising from beam bending and is given by[12]

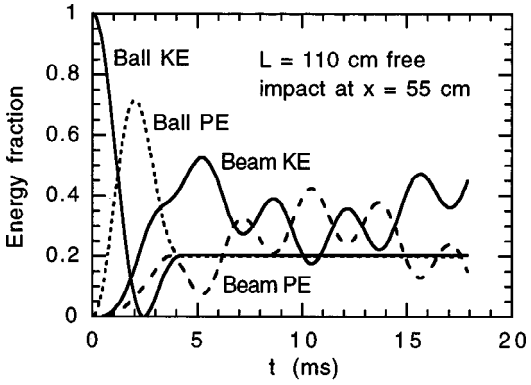

Fig. 9. The distribution of energy following an impact of the superball on the $L=110$-cm, $a=6$-mm freely supported beam for an impact in the center of the beam.

$$U=\int_0^L \frac{EI}{2}\left(\frac{d^2y}{dx^2}\right)^2 dx. \tag{13}$$

Most of the initial energy of the ball is rapidly converted to potential energy of the ball as a result of its compression. As the ball expands, some of this energy is dissipated in the ball and the rest is distributed as shown in Figs. 9 and 10. It is coincidental that the energy dissipated in the ball is almost identical to the kinetic energy of the ball after the collision. For an impact at the center of the beam, the beam recoils with a time-averaged stored potential energy slightly smaller than the time-averaged kinetic energy. For the impact at 90 cm, the ball rebounds with almost the same speed as an impact at the center, but the kinetic energy transferred to the beam is increased, and the stored PE in the beam is decreased, as expected from the conservation equations. At least that is the situation that evolves well after the collision is over.

As shown in Figs. 9 and 10, the distribution of energy between ''Beam KE'' and ''Beam PE'' does not depend significantly on the impact point during the collision itself. Consequently, the ball rebounds with essentially the same speed, regardless of the impact location, while the beam dynamics evolves with time, and continues to evolve after the ball has lost contact with the beam. After several transits of the impulse up and down the beam, it is then possible to interpret the motion of the beam in terms of rigid body dynamics. The

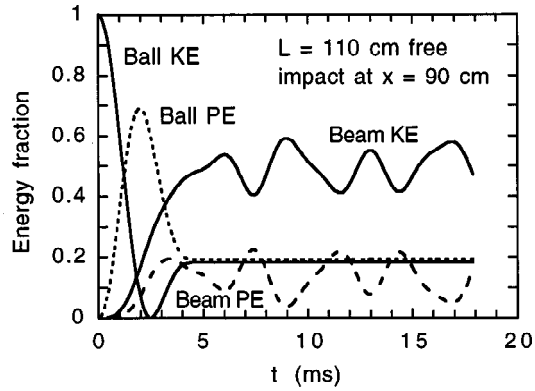

Fig. 10. The distribution of energy following an impact of the superball on the $L=110$-cm, $a=6$-mm freely supported beam for an impact 20 cm from one end of the beam.

mode frequencies and node locations in Figs. 9 and 10 are consistent with beam theory (more obviously when the calculations are extended over several fundamental vibration periods) but the frequencies appear to be twice as high since the vibrational energy components are a maximum twice each cycle.

The vibrational energy stored in the beam can be calculated for each impact point using Eq. (13), but this is time consuming since the calculations must extend over several fundamental vibration periods to determine the time-averaged vibrational energy. A simpler approach is to integrate the flexible beam equations only during the impact period to determine $e=v_2/v_1$ and the energy dissipated in the ball, and then use the rigid body Eqs. (11) and (12) to determine the fractional energy loss, f. The result for a tennis racket is described in Sec. IX.

IX. RELEVANCE TO A REAL TENNIS RACKET

The beam parameters chosen for this experiment do not accurately model the parameters of real bats or rackets, but they are not wildly different. Nevertheless, it is of interest to consider more realistic parameters. Consider, for example, a graphite/epoxy composite tennis racket of length $L=72$ cm, mass $M=320$ g, and thickness $a=20$ mm. The fundamental vibration frequency of such a racket, when freely suspended by a length of string, is typically about 125 Hz (period $T=8$ ms). Despite the fact that the racket head is round, the frame is hollow, and the ball impacts on almost massless strings, the vibration modes and the node locations of such a racket can be accurately modeled by assuming that the racket behaves as a uniform beam. The zero frequency dynamics of the racket (i.e., its rotation, translation, and the location of the center of percussion) can also be modeled in terms of a uniform beam, provided the ball impacts the strings on the long axis through the handle. An off-axis impact will cause the racket to rotate about the long axis, in which case the relevant moment of inertia is considerably larger than that of a uniform, rectangular cross-section beam of the same mass, length, and thickness as the racket. From Eq. (5), the relevant value of E/ρ for the racket is $1\times10^7\ \mathrm{N\,m\,kg^{-1}}$. This value of E/ρ is about a factor of 6 smaller than that observed for a straight graphite composite tube, and reflects the fact that the racket is loaded by the strings, the grip, a heavy coat of paint, and other reinforcement material, and also indicates that the carbon fibers are not all aligned in the same direction, but are woven into a braided cloth.

The rules of tennis specify that a tennis ball must have a mass of 57 g, a spring constant $k\sim2\times10^4\ \mathrm{N\,m^{-1}}$, and a coefficient of restitution (COR) of 0.74 when dropped from a height of 100 in. onto a concrete slab, with only small variations permitted. In this case, the ACOR is the same as the COR since the slab remains at rest. The ball therefore loses about 45% of its initial energy when dropped onto a concrete slab. In normal play, the ball does not impact on concrete or even on the racket frame. The impact is cushioned by the strings, with the result that the ball compression is reduced and hence the ball loss is less than that for an impact on concrete. When a ball is dropped onto the strings, and the head is clamped, the ball rebounds to about 70%–80% of its drop height, depending on the string tension, the ball speed, and the condition of the ball. Essentially all of the energy absorbed by the strings is given back to the ball.[13] In the calculations presented below, it is assumed that the bounce

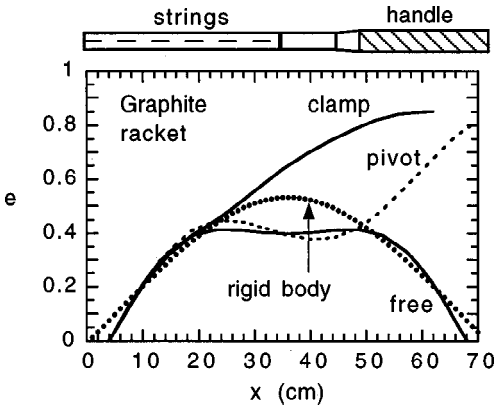

Fig. 11. Theoretical estimates of the ACOR for a graphite tennis racket of length 72 cm, mass 320 g, and thickness 20 mm. The tip of the racket, at $x=0$, is freely supported. The handle is either freely supported, pivoted at $x=72$ cm, or rigidly clamped between $x=62$ cm and $x=72$ cm. Also shown is a rigid body solution for the freely suspended racket, with $f=0.3$. The racket strings extend typically from $x=1$ cm to about $x=34$ cm.

height is 72%, corresponding either to a ''used'' ball impacting at low speed or a new ball impacting at relatively high speed. The hysteresis losses can be modeled, as described above, using $k_1=2\times10^4\ \mathrm{N\,m^{-1}}$ and $e^2=0.72$ or $e=0.85$, in which case $m=1$ and $n=1.768$. The relevant compression and energy loss when the racket head is free to recoil is governed by the relations $F=k_1(y_b-y_n)$ during the compression phase and $F=k_2(y_b-y_n)^{1.768}$ during the expansion phase.

The impact force acts via the strings over the whole racket head, but not instantaneously since there is a finite propagation delay, of order 0.5 ms, through the strings. It is assumed in the calculations presented below that the ball impacts on only one of the N segments, since the force is transmitted to its nearest neighbors, with a time delay comparable with that through the strings, as a result of beam bending. Further details of the collision would require a two-dimensional model of the racket head to take into account the two-dimensional nature of wave propagation through the strings as well as the frame.

Calculations of the ACOR for the above racket and ball parameters are shown in Fig. 11, for conditions where the racket is (a) freely suspended or (b) rigidly clamped over a 10 cm length at the end of the handle or (c) pivoted about an axis through the end of the handle. The length of the clamped racket is reduced, by the clamp, to 62 cm. In practice, the hand does not act as a rigid clamp, since the racket and the hand pivot about an axis through the wrist.[7] The boundary conditions at a pivot end are given by $y=0$ and $\partial^2y/\partial x^2=0$ since the displacement and the bending moment are both zero at a pivot (or ''pinned'') joint.

The racket results are surprising since the ACOR near the center of the racket is strongly affected by wave reflection from the clamped end, but not by reflections from the same end when that end is free or pivoted. This result is not simply due to the fact that the clamped racket is 10 cm shorter than the other rackets. The clamped racket has almost the same length and mass as the 60-cm aluminum beam shown in Fig. 6. The difference is that the racket is slightly stiffer, having a higher fundamental vibration frequency (125 Hz for the free racket and 87 Hz for the free aluminum beam) and the ball contact time is slightly longer (6.2 ms for the tennis ball and

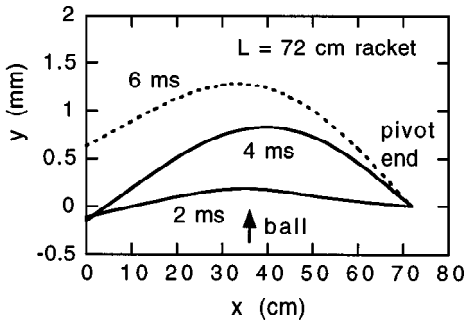

Fig. 12. Snapshots of the racket at 2-ms time intervals when the handle is pivoted at the end of the handle and the ball impacts at $x=36$ cm at $v_1=1.0\ \mathrm{ms^{-1}}$.

4.2 ms for the superball). The reflected pulse from the clamped end of the racket catches up with the ball as it is about to rebound, and ejects the ball at a relatively high speed. Furthermore, the contact duration is extended to 6.2 ms by this effect. In the case of the free or pivoted racket, reflections from either end take slightly longer to reach the ball due to the additional 10 cm racket length. When the reflection does reach the ball, the racket moves away from the ball, with the result that the contact time is reduced to about 5.2 ms, compared with 5.5 ms for an impact on a rigid surface. The dynamics are illustrated in Figs. 12 and 13, showing snapshots of the racket at 2-ms intervals after the initial impact.

The ''slingshot'' effect of the reflected pulse from a clamped end is mainly of academic interest since the hand and wrist act more like a pivot joint than a rigid clamp and since the ball normally impacts in a region about 10–25 cm from the tip of the racket, rather than near the center of the racket (i.e., about 36 cm from the tip) or near the clamped end. Consequently, the main significance of the results shown in Fig. 11 is that, for an impact on the strings, the behavior of the ball is almost totally independent of the method of support of the handle. There is only a marginal difference in the ACOR, about 20–30 cm from the tip of the racket, between a freely supported racket and one that is pivoted at the end of the handle.

Also shown in Fig. 11 is a rigid body calculation for this racket, assuming that it is freely suspended and that the fractional energy loss $f=0.3$. This value of f was chosen to give a reasonable fit to the flexible racket solutions. The fit agrees moderately well with the flexible racket results, except near the tip and the throat of the racket since vibration losses act

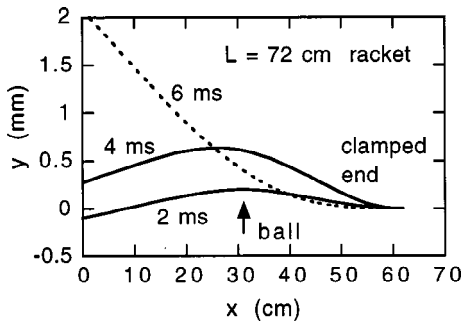

Fig. 13. Snapshots of the racket at 2-ms time intervals when the handle is clamped between $x=62$ cm and $x=72$ cm and the ball impacts at $x=31$ cm at $v_1=1.0\ \mathrm{ms^{-1}}$.

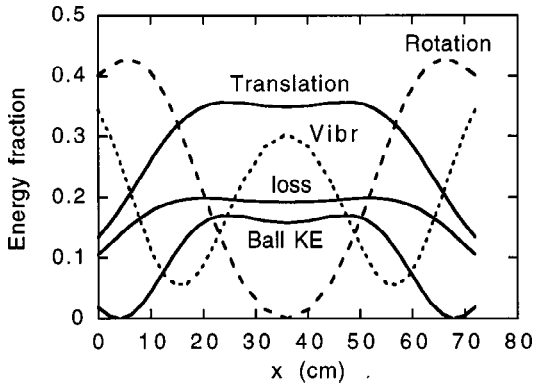

Fig. 14. A forced rigid body fit to the flexible beam solutions for the freely suspended graphite racket. The distribution of the initial ball energy is plotted as a function of the impact distance, x, from the tip of the racket. Each curve is normalized to the initial energy $0.5m_b v_1^2$. The ''loss'' curve is the fraction of this energy dissipated in the ball. The ''Vibr'' curve is the fraction stored in racket vibrations. The various energy fractions sum to unity. In practice, the only region of interest is $3<x<30$ cm, corresponding to an impact on the strings.

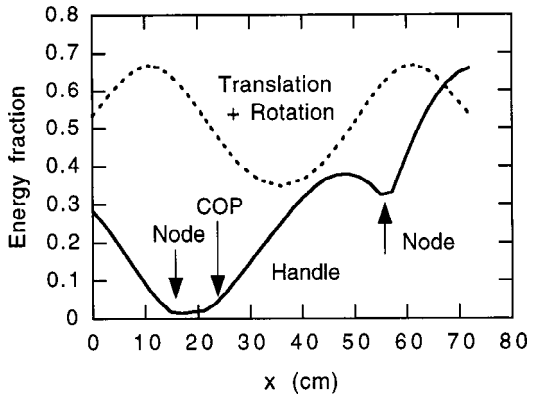

Fig. 15. The sum of the translational and rotational energy fractions in Fig. 14 is shown by the dashed curve. The solid curve shows the fraction of the initial ball energy that is transferred to the handle, as a function of the impact distance, x, from the tip of the racket. The node points correspond to nodes of the fundamental mode, and the COP at $x=24$ cm is shown for a conjugate point at the end of the handle.

to increase f in these locations. A ''forced'' rigid body fit to the flexible racket solutions, for an impact on the freely suspended racket, is shown in Fig. 14. The ball loss due to hysteresis, and the ACOR, were calculated using the flexible beam model. The fractional energy loss, f, was then determined from Eqs. (11) and (12). The translational and rotational energies of the racket were determined, from the known value of $e=v_2/v_1$, with the aid of Eqs. (8) and (9). The energy stored in racket vibrations, normalized to the initial ball energy, was obtained by subtracting the normalized ball loss from f.

As shown in Fig. 14, the energy dissipated in the ball is actually less than that when the head is rigidly clamped (for the same incident ball speed) since the racket frame, as well as the strings, absorbs some of the impact energy. As a result, the ball compresses by a smaller amount, and the hysteresis loss is reduced. The vibrational energy stored in the racket passes through a broad minimum for an impact at the fundamental vibration node. It is not zero, since other modes are excited at this location, but the fundamental mode is clearly the most significant. For a uniform beam, the nodes of the fundamental mode are located at $x/L=0.22$ and $x/L=0.78$, or at $x=16$ cm and $x=56$ cm for the $L=72$-cm racket. For a racket, the fundamental node is close to the middle of the strings. One might therefore expect a significant localized increase in the ACOR for an impact in the middle of the strings. Such an effect is not observed, despite the reduction in the energy coupled to racket vibrations at the node, since the kinetic energy coupled to the racket passes through a broad maximum near the node point. This effect is shown in Fig. 15, where the sum of the translational and rotational energy fraction curves is plotted as a function of the impact point. Alternatively, one can argue that the ball does not ''know'' that it struck a node until after the collision is over. The impulse must propagate to both ends of the racket and back in order for a node point to be established.

Also shown in Fig. 15 is a plot of the kinetic energy transferred to the handle, for the freely suspended racket. This result was obtained by summing the kinetic energy of all segments in the last 10 cm of the handle, and recording the maximum value of the kinetic energy during the 30-ms period following the impact. The energy stored in the handle as a result of local beam bending was found to be neglible. However, the handle still vibrates after the impact due to the vibrational energy stored in other parts of the racket. It might appear from Fig. 15 that, for impacts near the end of the handle, more energy is stored in the handle than in the whole racket. However, the translational plus rotational energy curve represents the time average energy, with the vibrational component removed, whereas the handle energy curve shows the peak energy in the handle, including the vibrational energy. The most significant feature of the handle energy curve is that the handle energy is minimized for an impact in the region from about $x=14$ cm to about $x=21$ cm. This can be attributed to the fact that (a) the vibrational energy is minimized for an impact at the fundamental vibration node (at $x=16$ cm) and (b) the time average kinetic energy drops to zero at any given point in the handle for an impact at the corresponding center of percussion (COP) on the strings.[6,7] For conjugate points between the end of the handle and 10 cm from the end of the handle, the corresponding COP points extend from $x=19.4$ cm to $x=24.0$ cm. Consequently, the ''sweet spot'' zone, representing a region where shock and vibration transferred from the handle to the player are minimized, corresponds to impacts near or between the fundamental node point and the COP points.

Manufacturers have strived for many years to produce a perfectly rigid racket since the vibration losses would then be zero. Modern graphite rackets are certainly much stiffer than the older generation of wood or aluminum rackets, but they are not infinitely stiff. In fact, they do not need to be. If E is increased by a factor of 3, keeping the racket mass, length, and thickness fixed, the flexible racket solution is almost identical to the rigid body solution shown in Fig. 11. If E is reduced by a factor of 3, e is decreased by about 20% along the whole length of the racket. Consequently, only marginal gains can be obtained by increasing the stiffness of modern rackets.

X. CONCLUSIONS

In this paper, aluminum beams of different length and thickness were used to simulate the behavior of a ball collid-

ing with a baseball bat or a tennis racket. It was found that the apparent coefficient of restitution, for an impact at any point well removed from either end of the beam, is independent of the impact location or the length of the beam or the method of support at the ends. These results support the often-quoted assumption that the impulsive reaction force on the handle can be neglected. A rigid body model of the collision yields results that are, in general, only roughly consistent with experimental data or with solutions obtained for a flexible beam. The rigid body model works best when the duration of the collision is greater than the vibration period of the fundamental mode of the freely supported beam. However, the rigid body model must be supplemented with independent estimates of the energy stored in vibrational modes. The flexible beam model is superior and yields results that are in remarkably good agreement with experimental data, at least for a uniform beam. One can therefore expect that an extension of the model to treat real, nonuniform bats and rackets will yield similarly reliable results.

The mechanics of a bat and ball collision can be pictured in the following simplified terms. During the collision, the bat bends locally by an amount that is independent of the impact point, provided the impact is not too close to the end of the bat. The impact generates a pulse that propagates to each end of the bat and returns to the impact point either before or after the ball has rebounded, depending on the flexibility of the ball, the flexibility of the bat, and the distance to each end. If the reflected pulses arrive after the ball rebounds, then the ball has no way of ''knowing'' where it landed and the rebound speed is independent of the impact point. Similarly, the beam does not ''know'' if it was struck in the middle or at any of the vibration nodes until well after the collision is over. After the ball has lost contact with the bat, the pulse propagates up and down the bat and distributes the impact energy in a manner that is governed by the conservation equations for linear and angular momentum or in a manner that can be calculated in terms of the normal modes, including the zero frequency modes.[5,9] An experimentalist could measure the amplitudes of the various modes after the collision is over, calculate the energy in the modes, and then use the conservation equations to calculate the rebound speed of the ball. However, it would be simpler to measure the rebound speed directly. In this sense, a rigid body model of the collision is of limited use in determining the rebound speed of the ball.

ACKNOWLEDGMENTS

It is a pleasure to acknowledge stimulating discussions with Professor Howard Brody and Professor Alan Nathan.

APPENDIX

A finite difference form of Eq. (2) can be obtained by reference to Fig. 16. The beam is approximated as N segments each of mass m, separated by a distance s in the x direction. If the nth segment is displaced in the y direction by an amount y_n, then

$$y'_{n-0.5}=(dy/dx)_{n-0.5}=(y_n-y_{n-1})/s$$

and

$$y'_{n+0.5}=(dy/dx)_{n+0.5}=(y_{n+1}-y_n)/s.$$

Hence,

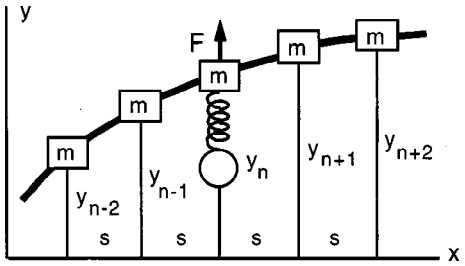

Fig. 16. Discrete segment model for a uniform beam. The ball exerts a force F on the nth segment and can be treated as a simple or as a nonlinear and lossy spring.

$$y''_n=(d^2y/dx^2)_n=(y'_{n+0.5}-y'_{n-0.5})/s$$
$$=(y_{n+1}-2y_n+y_{n-1})/s^2.$$

Similarly,

$$\left(\frac{d^4y}{dx^4}\right)_n=\frac{y''_{n+1}-2y''_n+y''_{n-1}}{s^2}$$
$$=\frac{(y_{n+2}-4y_{n+1}+6y_n-4y_{n-1}+y_{n-2})}{s^4}.$$

The time derivatives can be expressed in an analogous form using equal increments, Δt, in time. Given the values y_{t-1}, y_t, and $y''_t=(d^2y/dt^2)$, then $y_{t+1}=2y_t-y_{t-1}+(\Delta t)^2y''_t$. At each time step, y_{t+1} is evaluated for each segment, then the x derivatives are reevaluated prior to the next time step. However, this procedure cannot be applied to the first two or the last two segments at the ends of the beam since the x derivative at any given segment is expressed in terms of the y displacement of the two segments on either side of the given segment. The y displacement of the end segments was obtained by imposing the relevant boundary conditions as described above. For example, at a free end, $y_2-y_1=y_3-y_2=y_4-y_3$. At a clamped end, $y_1=y_2=0$. At a pivot joint, $y_1=0$ and $y_2=y_3/2$. These boundary conditions extend over a small but finite length of the beam and effectively reduce the beam length, especially if the number of segments is small. Ideally, the boundary conditions apply to only one point at the very end of the beam. Consequently, a small ''end correction'' was used in the numerical solutions by allowing the numerical beam to be two segments longer than the actual beam. However, in order to satisfy the energy conservation equations, it was necessary to assume that the end segments had zero mass. For the other segments, $s=L/(N-2)$ and $m=M/(N-2)$. Good agreement with the analytical eigenmode frequencies was obtained using $N\sim 40$ segments.

The response of a beam to any given impulse consists, in theory, of an infinite set of eigenmodes. In principle, numerical integration of Eqs. (2) and (3) would therefore require infinitesimal time steps to resolve all modes. In practice, it was found that time steps of order 10 μs provided sufficient accuracy since the impulse duration, typically about 5 ms, was too long to excite modes of frequency greater than about 300 Hz and since the division of the beam into N discrete segments eliminated modes of wavelength shorter than the segment separation s. Experimentally, very high frequency

modes are of no consequence since they are heavily damped and since the frequency spectrum of an impulse of duration τ extends only to about $f=1/\tau$.

[1]H. Brody, ''The sweet spot of a baseball bat,'' Am. J. Phys. **54**, 640–643 (1986).
[2]D. C. Leigh and W-L. Lu, ''Dynamics of interaction between ball, strings and racket,'' Int. J. Sports Biomechanics **8**, 181–206 (1992).
[3]G. Watts and A. T. Bahill, *Keep your Eye on the Ball, the Science and Folklore of Baseball* (Freeman, New York, 1990), pp. 102–125.
[4]H. Brody, ''The physics of tennis. III. The ball–racket interaction,'' Am. J. Phys. **65**, 981–987 (1997).
[5]L. L. Van Zandt, ''The dynamical theory of the baseball bat,'' Am. J. Phys. **60**, 172–181 (1992).
[6]R. Cross, ''The sweet spot of a baseball bat,'' Am. J. Phys. **66**, 772–779 (1998).
[7]R. Cross, ''The sweet spots of a tennis racket,'' Sports Eng. **1** (2), 63–78 (1998).
[8]K. F. Graff, *Wave Motion in Elastic Solids* (Oxford U.P., Oxford, 1975), pp. 140–210.
[9]W. Goldsmith, *Impact* (Arnold, London, 1960), pp. 108–129.
[10]H. Brody, ''Physics of the tennis racket,'' Am. J. Phys. **47**, 482–487 (1979).
[11]R. Cross, ''The bounce of a ball,'' Am. J. Phys. **67**, 222–227 (1999).
[12]S. P. Timoshenko and D. H. Young, *Elements of Strength of Materials* (Van Nostrand, Princeton, 1968), 5th ed., p. 220.
[13]H. Brody, ''How would a physicist design a tennis racket?'' Phys. Today **48**, 26–31 (March 1995).

TO FATHOM OR TO USE

By 1896 the field of electrical engineering had split from physics. Physicists certainly failed to heed this author's advice, and now must attempt to fathom four subtle and mighty forces, not two.

''**INTRODUCTION**

The great forces of the world are invisible and impalpable; we cannot grasp or handle them; and though they are real enough they have the appearance of being very unreal. Electricity and Gravity are as subtle as they are mighty: they elude the eye and hand of the most skillful philosopher. In view of this, it is well for the average man not to try to fathom, too deeply, the science of either; neither Edison or Tesla have done that yet.

To take the machines and appliances as they are ''on the market'' and to acquire the skill to operate them, is the longest step toward the reason for doing it, and why the desired results follow—thus working on the natural method of judging causes from effects.''

N. Hawkins, *New Catechism of Electricitiy: A Practical Treatise* (Theo. Audel & Co., New York, 1896), p. xv.